Detailed Dynamics of the Photodissociation of Cyclobutane

Yusheng Dou,*,†,‡ Yibo Lei,†,§ Anyang Li,† Zhenyi Wen,†,§ Ben R. Torralva,# Glenn V. Lo,‡ and Roland E. Allen⊥

Bio-Informatics Institute, Chongqing University of Posts and Telecommunications, Chongqing, 400065, People's Republic of China, Department of Physical Sciences, Nicholls State University, P.O. Box 2022, Thibodaux, Louisiana 70310, Modern Physical Institute, Northwest University, Xi'an, 710069, People's Republic of China, Chemistry and Materials Science, Lawrence Livermore National Laboratory, Livermore, California 94550, and Department of Physics, Texas A&M University, College Station, Texas 77843

Received: September 29, 2006; In Final Form: December 4, 2006

Semiclassical electron-radiation-ion dynamics simulations are reported for the photodissociation of cyclobutane into two molecules of ethylene. The results clearly show the formation of the tetramethylene intermediate diradical, with dissociation completed in ∼400 fs. In addition, the potential energy surfaces of the electronic ground state and lowest excited-state were calculated at the complete-active-space self-consistent-field/multireference second-order perturbation theory (CASSCF/MRPT2) level with 6-31G* basis sets, along the reaction path determined by the dynamics simulations. There are well-defined energy minima and maxima in the intermediate state region. It is found that both C−C−C bond bending and rotation of the molecule (around the central C−C bond) have important roles in determining the features of the potential energy surfaces for the intermediate species. Finally, the simulations and potential energy surface calculations are applied together in a discussion of the full mechanism for cyclobutane photodissociation.

Introduction

The dissociation of cyclobutane to form two molecules of ethylene (or the reverse process) is a textbook example of an addition/elimination reaction that involves the Woodward−Hoffmann rules,[1] and it has been well-studied both experimentally and theoretically.[2] Two different mechanisms were proposed. In the first scenario, the reaction proceeds directly through a transition state at the saddle point of the activation barrier. In the second scenario, it proceeds through a two-step process, with one of the C−C bonds first breaking to form tetramethylene (a diradical reaction intermediate), which then passes through a transition state, finally yielding two molecules of ethylene.

Thermodynamic analysis of appropriately substituted precursors,[3−7] as well as of the cycloaddition of ethylene to form butane,[8] suggested the existence of the diradical intermediate. The development of techniques based on ultrashort laser pulses finally made it possible to study the dynamics of the intermediates in chemical reactions directly: Using femtosecond laser techniques, together with time-of-flight mass spectrometry (TOF MS) in a molecular beam, Zewail and co-workers identified the reactive immediate, the tetramethylene diradical, in the transition state on a real-time scale.[9,10] In their experiments, the diradicals are produced by the decarbonylation of cyclopentanone initiated by a femtosecond-scale laser pulse. It has been found that the tetramethylene diradical immediate decays at 340, 700, or 840 fs, depending on the total energy used.

Many quantum calculations at different levels have been performed[11−21] to locate the minimum and saddle points of the potential energy surface for the electronic ground state of tetramethylene. Various calculations have yielded somewhat controversial results regarding the existence of energy wells near the transition state of the reaction. Calculations at the complete-active-space self-consistent-field (CASSCF) level suggest[13,14] that there are two minima and six saddle points on the potential energy surface of tetramethylene. Computations at a higher level (for example, with the MR-AQCC approximation) indicate[21] that these stationary points and their relative energies are significantly dependent on the level of theory applied. Note that the stationary points studied in these investigations are mainly along a reaction path that involves only rotation of the diradical about the central C−C bond or dissociation of the second C−C bond. Few of them include terminal CH_2 twist motion.[21]

Here we report studies that use both (i) semiclassical electron-radiation-ion dynamics (SERID), which is a technique for simulations of the electronic and nuclear dynamics following an applied laser pulse,[22,23] and (ii) calculations of the potential energy surfaces for the electronic ground state and lowest excited state at the complete-active-space self-consistent-field/multireference second-order perturbation theory (CASSCF/MRPT2) level with 6-31G* basis sets. We will first discuss our SERID simulations of the ring opening reaction of cyclobutane to form two molecules of ethylene. The results of these simulations provide a microscopic picture of the formation of the tetramethylene diradical immediate and detailed information on its dynamics. We will then consider the potential energy surfaces, following the reaction path from reactant to product, as determined by the simulation. The electronic ground-state potential energy surface is found to show rather well-defined

* Author to whom correspondence should be addressed. Tel.: 985-448-4880. Fax: 985-448-4641. E-mail: Yusheng.Dou@nicholls.edu.

† Bio-Informatics Institute, Chongqing University of Posts and Telecommunications.

‡ Department of Physical Sciences, Nicholls State University.

§ Modern Physical Institute, Northwest University.

Chemistry and Materials Science, Lawrence Livermore National Laboratory.

⊥ Department of Physics, Texas A&M University.

10.1021/jp066422y CCC: $37.00
Published on Web 01/25/2007

energy wells. The potential energy surfaces calculated in this way involve all the nuclear degrees of freedom and allow us to investigate how the reaction pathway, particularly near the transition state, is affected by different internal coordinates.

Methodology

In our semiclassical electron-radiation-ion dynamics approach, the time-dependent quantum states are calculated for the valence electrons; however, both the radiation field and the motion of the nuclei are treated classically. As one can see from time-dependent perturbation theory, such a semiclassical treatment effectively includes effective "*n*-photon" and "*n*-phonon" processes in absorption and stimulated emission. This fact permits us to examine nontrivial processes such as multielectron and multiphoton excitations, the indirect excitation of vibrational modes, intramolecular vibrational energy redistribution, and interdependence of the various electronic and vibrational degrees of freedom.

A detailed description of this method has been published elsewhere;[22,23] therefore, only a brief outline is given here. The one-electron states are updated at each time step by solving the time-dependent Schrödinger equation in a nonorthogonal basis:

$$i\hbar\frac{\partial\Psi_j}{\partial t} = \mathbf{S}^{-1}\cdot\mathbf{H}\cdot\Psi_j \tag{1}$$

where **S** is the overlap matrix for the atomic orbitals. The electrons are coupled to the vector potential **A** of the radiation field through the time-dependent Peierls substitution:[24]

$$H_{ab}(\mathbf{X}-\mathbf{X}') = H^0_{ab}(\mathbf{X}-\mathbf{X}')\exp\left[\frac{iq}{\hbar c}\mathbf{A}\cdot(\mathbf{X}-\mathbf{X}')\right] \tag{2}$$

Here, $H_{ab}(\mathbf{X}-\mathbf{X}')$ is the Hamiltonian matrix element for basis functions *a* and *b* on atoms with position vectors **X** and **X′**, respectively, and *q* is the charge of the electron ($q = -e$).

The Hamiltonian matrix, overlap matrix, and effective nuclear−nuclear repulsion are based on density-functional calculations.[25] In our previous investigations of C_{60} responding to laser pulses of various intensities,[26] and of the photocyclization of *cis*-stilbene to dihydrophenanthrene,[27] this same model was found to yield a very good description of C−C bond cleavage and closure.

The nuclear motion is determined by the Ehrenfest equation of motion:

$$M_l\frac{\mathrm{d}^2X_{l\alpha}}{\mathrm{d}t^2} = -\frac{1}{2}\sum_j\Psi_j^+\cdot\left(\frac{\partial\mathbf{H}}{\partial X_{l\alpha}} - i\hbar\left(\frac{1}{2}\right)\left(\frac{\partial\mathbf{S}}{\partial X_{l\alpha}}\right)\cdot\frac{\partial}{\partial t}\right)\cdot\Psi_j - \frac{\partial U_{\mathrm{rep}}}{\partial X_{l\alpha}} \tag{3}$$

where U_{rep} is the effective nuclear−nuclear repulsive potential. Here, $X_{l\alpha} = \langle\hat{X}_{l\alpha}\rangle$ is the expectation value of the time-dependent Heisenberg operator corresponding to the α coordinate of the nucleus labeled by *l* (with $\alpha = x,y,z$). The replacement of the exact Ehrenfest theorem by eq 3 requires a single approximation. Terms of the second order and higher in the quantum fluctuations $\hat{X} - \langle\hat{X}_{l\alpha}\rangle$ are neglected on the right-hand side of the equation. (This can be seen by writing $\{\partial\hat{H}\}/\{\partial\hat{X}_{l\alpha}\}$ as a Taylor series expansion in $\hat{X} - \langle\hat{X}_{l\alpha}\rangle$, in the original Heisenberg equation of motion for $\hat{X}$, and then taking the expectation value of both sides of the equation to obtain eq 3 after terms of order $(\hat{X} - \langle\hat{X}_{l\alpha}\rangle)^2$ are neglected.) Because these fluctuations, in the present context, are typically <0.05 Å for carbon and <0.10 Å even for hydrogen, the use of eq 3 is a rather good approximation in the present context of simple atomic motion on a time scale of a few picoseconds. (There are other contexts, of course, where the quantum behavior of nuclei can be important. For example, tunneling of H atoms can have a role in other types of reactions, or on longer time scales, and the proper quantization of vibrational states is certainly very important in spectroscopy.) Because the wavepacket for a nucleus is small, compared to the size of an atom, there is little tendency for this wavepacket to "pull apart" under the influence of electronic forces and result in more than one trajectory during the processes studied here. In addition, one expects quantum fluctuations and classical fluctuations to result in essentially the same type of qualitative behavior (within the present context); therefore, the same multiple trajectories that might result from quantum fluctuations can already be seen in our classical simulations.

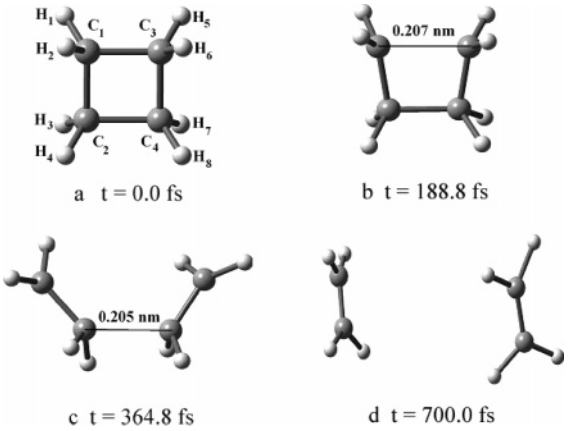

Figure 1. Snapshots from semiclassical dynamics simulation of the photodissociation of cyclobutane to form two ethylene molecules. Note that the first C−C bond is broken after ~190 fs, and the second after ~365 fs. (An animation file for this reaction is available at http://www.nicholls.edu/phsc/ydou/ring_opening_cyclobutane.htm.)

The time-dependent Schrödinger equation (eq 1) is solved using a unitary algorithm that is based on the equation for the time evolution operator.[28] Equation 3 is numerically integrated with the velocity Verlet algorithm (which preserves phase space). A time step of 50 as (where as rerpesents attoseconds) was used, because this yielded satisfactory energy conservation. We list a few details to indicate the computational requirements: Four parallel processors were used on an SGI model Altix 3700, and a 1-ps run requires ~3 CPU hours. A few tens of simulations have been run with different choices for laser parameters, such as fluence and duration, to obtain a clear example of the process being studied.

As mentioned previously, the Hamiltonian and effective nuclear repulsion used in eqs 1 and 3 are density-functional-based.[25,26] For example, the elements of the Hamiltonian matrix, in a basis with *s* and *p* atomic orbitals, are determined as a function of the internuclear distances by the parameters calculated through the procedure described in ref 25. The limitations of local density functional methods lead to excitation energies that are not quantitatively accurate, but the bond lengths and vibrational frequencies obtained are rather reliable. As mentioned previously, the present model has been successful in many previous applications, including those of refs 26 and 27.

As indicated in Figure 1a, all nuclear degrees of freedom are included in the calculation. Before the cyclobutane molecule is coupled to the vector potential, it is given a puckered geometry and allowed 1000 fs to relax to its optimized ground-state geometry at a temperature of 300 K. The laser pulse was taken to have a full width at half-maximum (fwhm) duration of 100

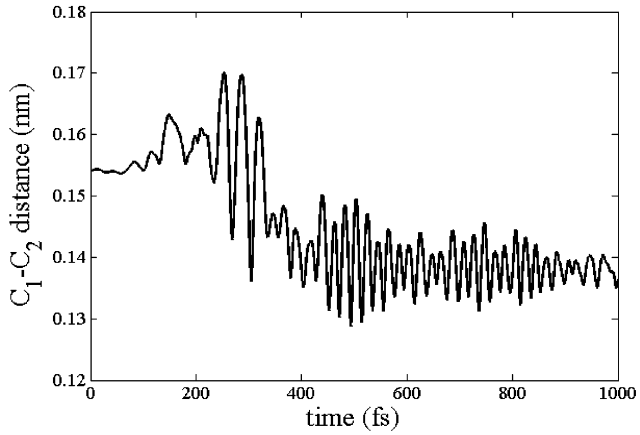

Figure 2. Time dependence of a C−C bond ultimately associated with one ethylene molecule. Notice that this bond begins to shorten in the intermediate state, and it becomes a double bond after dissociation.

fs (with a profile that is very almost Gaussian[28]), a fluence of 0.90 kJ/m^2, and a wavelength corresponding to a photon energy of 6.50 eV. This wavelength matches the density-functional energy gap between the highest-occupied molecular orbital (HOMO) and lowesy unoccupied molecular orbital (LUMO) levels of cyclobutane. The fluence was chosen such that the forces on the nuclei are large enough to break two nonadjacent C−C bonds successively, but not large enough to break any C−H bond. A single trajectory was examined in the simulation.

The potential energy surfaces of both the electronic ground state and the first excited state were calculated at the CASSCF/MRPT2 level with 6-31G* basis sets, using the XIAN CI code[29] with no symmetry restriction, and with four electrons and four orbitals included in the active space. For tetramethylene, there are then states of the same symmetry and spin multiplicity, and we broke the degeneracy by including states outside the active space, labeled by the symbol "β". Initially, the energies and corresponding eigenvectors were obtained in standard CASSCF calculations:

$$\mathrm{E}_0^i, \Psi_0^i = \sum_{R \in CAS} \mathrm{C}_R^i \Phi_R \qquad (\text{for } i = 1, 2, ...) \tag{4}$$

Rayleigh−Schrödinger perturbation theory then was used to obtain the nondegenerate energies, using an iterative procedure:

$$\boldsymbol{E}^i = \boldsymbol{E}_0^i + \sum_{\beta \notin CAS} \frac{|\langle \Psi_0^i | H | \Phi_\beta \rangle|^2}{\boldsymbol{E}_0^i - \boldsymbol{E}_\beta} \tag{5}$$

In eq 5, $\boldsymbol{E}_\beta$ represents the energies calculated in the previous iteration.

Results and Discussion

Four snapshots from the simulation at different times are shown in Figure 1. Approximately 190 fs after the beginning of the laser pulse (which has a full duration of 200 fs), the C_1−C_3 bond is broken and the tetramethylene intermediate is formed. After ∼365 fs, the C_2−C_4 bond then is broken and two ethylene molecules are produced. The lifetime of the tetramethylene intermediate can be defined as the time until the second C−C bond is broken, and the value found in the simulation is thus comparable to the experimental value of 340 fs. After 450 fs, the two ethylenes move away from each other.

The variation of the C_1−C_2 bond with time is shown in Figure 2. This is a single bond in cyclobutane and becomes a double bond in ethylene. Starting at ∼0.155 nm, which is the length of a typical C−C single bond, the C_1−C_2 bond vibrates strongly after the laser pulse is applied. After 190 fs, its length decreases, but it is still longer than 0.135 nm, which is the length of a regular C−C double bond, because the diradical has formed. After 365 fs, with the dissociation into two ethylene molecules, this C_1−C_2 bond is finally shortened to ∼0.135 nm, and it remains at this length until the end of the simulation.

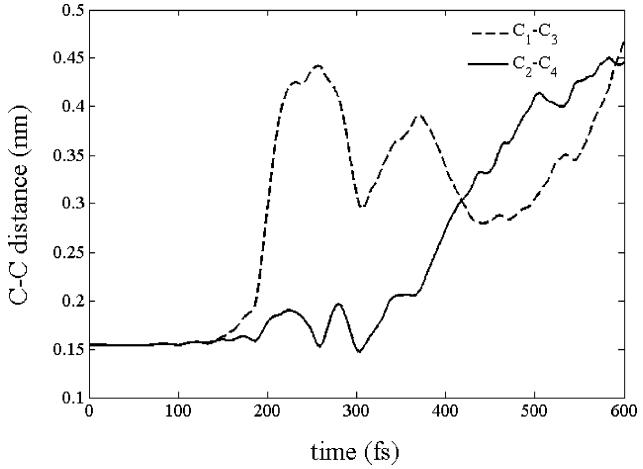

Figure 3. Time dependence of the C_1−C_3 and C_2−C_4 bonds. One can observe both the sequence of bond-breaking and the dynamics of the tetramethylene diradical intermediate.

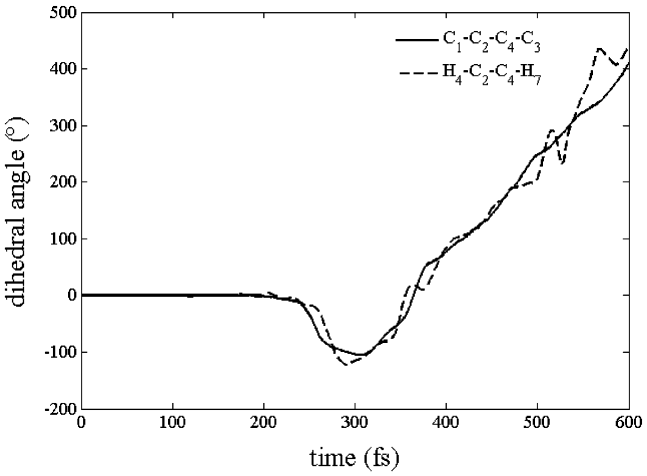

Figure 4. Changes in the dihedral angles C_1−C_2−C_4−C_3 and H_4−C_2−C_4−H_7 in tetramethylene. After ∼400 fs, the C_2−C_4 bond has been broken and the behavior of these angles is no longer physically meaningful.

The variations with time of the C_1−C_3 and C_2−C_4 distances are shown in Figure 3. The C_1−C_3 bond clearly breaks just before 200 fs and the C_2−C_4 bond dissociates not long after 350 fs. The variation of the C_1−C_3 distance between 200 fs and 350 fs exhibits dynamical features of the tetramethylene intermediate diradical associated with variations of the C_1−C_2−C_4−C_3 torsional angle and the C−C−C angles.

Figure 4 shows the time dependence of both the C_1−C_2−C_4−C_3 and the H_4−C_2−C_4−H_7 torsional angles. Neither varies significantly before ∼200 fs, when the tetramethylene intermediate diradical is formed. Starting from 0°, the diradical rotates about the C_2−C_4 bond during the next 100 fs to approximately −100°, and then turns back. It passes through 0° after ∼365 fs and continues trivially to increase after the C_2−C_4 bond is broken. The H_4−C_2−C_4−H_7 dihedral has a similar variation trend as the C_1−C_2−C_4−C_3 before ∼400 fs, at which point the

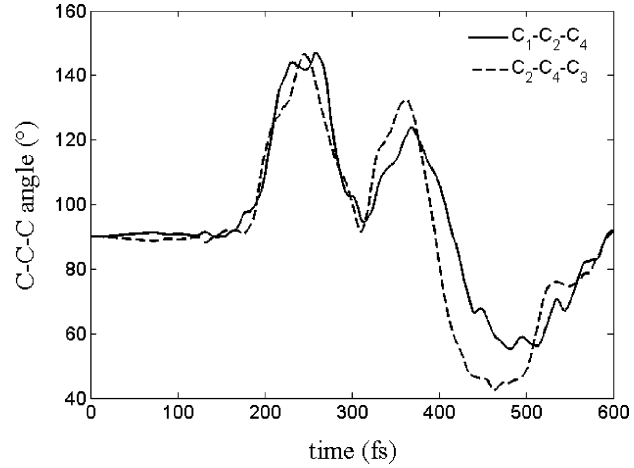

Figure 5. Variation with time of the $C_1-C_2-C_4$ and $C_2-C_4-C_3$ bond bending angles.

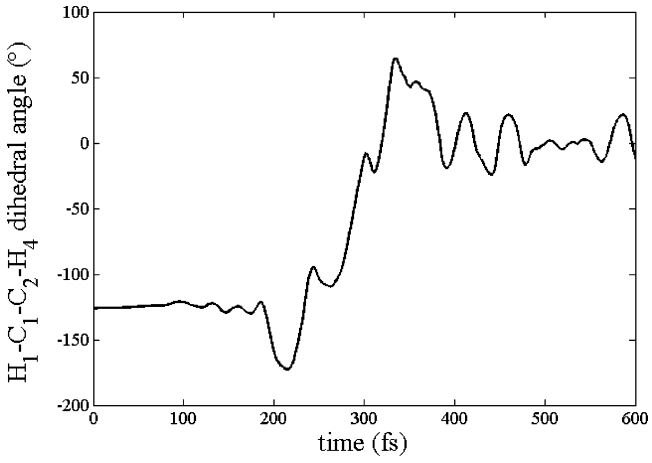

Figure 6. Changes in the dihedral angle $H_1-C_1-C_2-H_4$.

diradical dissociates into two ethylene molecules. The time dependence of the $C_1-C_2-C_4$ and $C_3-C_4-C_2$ angles is shown in Figure 5. Between 190 fs and 365 fs, one can see large-amplitude angle-bending vibrations, which result from the breaking of the C_1-C_3 bond to form the diradical.

Figure 6 shows the variations with time of the $H_1-C_1-C_2-H_4$ torsional angle, which rotates from $-180°$ to $0°$, with vibrations, while in the diradical configuration.

The variations with time of the HOMO and LUMO energies are presented in Figure 7, and the time-dependent population of the LUMO is shown in Figure 8. (Note that the HOMO and HOMO-1 of the cyclobutane ultimately evolve into two identical HOMOs of the ethylene molecules after dissociation, and the original LUMO and LUMO$+1$ similarly evolve into two identical LUMOs.) Figure 7 demonstrates the abrupt change in the HOMO and LUMO energies when the C_1-C_3 bond breaks, at $\sim$190 fs. There are two close approaches of these levels, with avoided crossings, with the energy separations being 0.111 eV at 197.6 fs and 0.106 eV at 250.4 fs. The coupling of the states at 197.6 fs produces only weak electronic transitions, as can be seen in Figure 8. On the other hand, the coupling at 250.4 fs results in the rather dramatic nonadiabatic transitions from LUMO to HOMO that can also be observed in Figure 8. Figure 8 shows that $\sim$0.7 electron is excited to the LUMO orbital until 200 fs when the laser pulse is turned off. Examination of the populations of HOMO and HOMO-1 levels indicate that the electrons populated in LUMO mainly come from HOMO, indicating a single excitation from the e_u orbital to the a_{2g} orbital. This should produce an electronic state E_u.

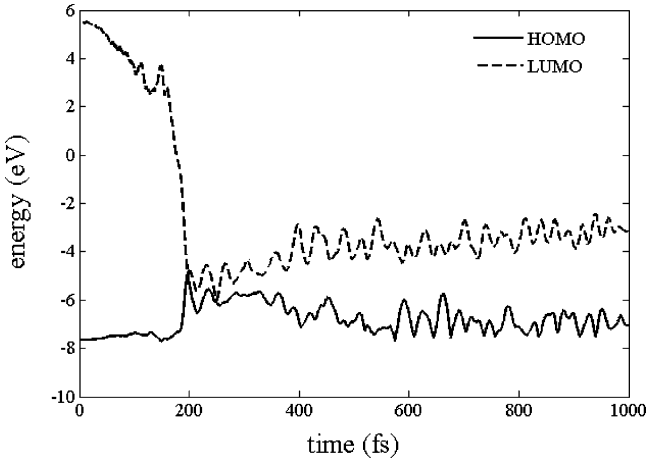

Figure 7. Variation with time of the HOMO and LUMO levels.

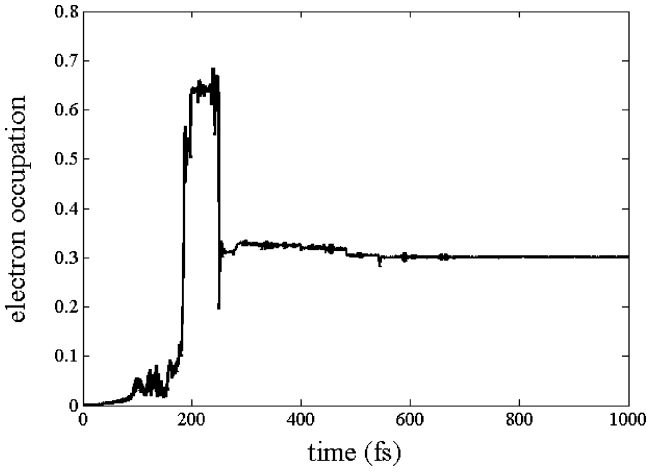

Figure 8. Time-dependent population of the LUMO.

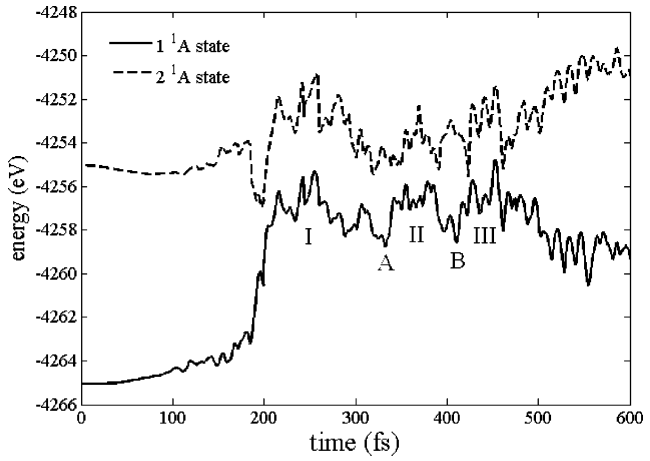

Figure 9. Potential energy surfaces (as defined in the text) for the electronic ground state and lowest excited state of the molecule, calculated at the CASSCF/MRPT2 level with 6-31G* basis sets. The nuclear positions in the molecule at each time step were determined in the semiclassical dynamics simulation described in the text.

To understand the dissociation process more completely, we have performed completely independent calculations of the total energy for both the ground state and the first excited state of the molecule, as a function of time, along the reaction path determined in the SERID simulation previously described. These calculations were performed at the CASSCF/MRPT2 level with 6-31G* basis sets, and the results are shown in Figure 9. (It should be emphasized that the curves of Figure 9 are one-

dimensional "potential energy surfaces", corresponding to the classical nuclear trajectories determined "on the fly" in a simulation, for which the electron-radiation-ion dynamics is given by eqs 1−3.) The results clearly indicate a reaction intermediate state, between ∼200 fs and 450 fs. There are two rather well-defined energy wells in the ground-state potential energy surface: one that is located at ∼330 fs (labeled "A"), and another at ∼410 fs (labeled "B"). Figures 5 and 9 show that the electronic ground-state potential energy surface is largely determined by variations in the C−C−C angles: The two energy wells are associated with C−C−C angles near 90° (the initial value in cyclobutane), whereas the higher-energy regions I, II, and III are associated with C−C−C angles that are substantially different from 90°. Figures 4 and 9 clearly show that the large deviation of the $C_1-C_2-C_4-C_3$ torsional angle from its initial value of 0° is also associated with the intermediate state of the molecule. We conclude that the C−C−C angles and the $C_1-C_2-C_4-C_3$ torsional angle are the main internal reaction coordinates that define the features of the ground-state potential energy surface in the intermediate-state region. Expansion of the C−C−C angle seems to increase the ground-state energy, whereas the rotation of the molecule about the C_2-C_4 bond (away from 0°) reduces it. The same is true of the first excited state, the behavior of which is also shown in Figure 9.

Conclusions

The combination of semiclassical electron-radiation-ion dynamics (SERID) simulations and complete-active-space self-consistent-field/multireference second-order perturbation theory (CASSCF/MRPT2) calculations of the potential energy surfaces (for the ground state and lowest excited state of the molecule while "on the fly") provides a clear picture of the mechanism for photodissociation of cyclobutane to form two molecules of ethylene. When a femtosecond-scale laser pulse is applied, there is a highest-occupied molecular orbital (HOMO) to lowest-unoccupied molecular orbital (LUMO) excitation during the first 200 fs, and one C−C bond breaks to form the intermediate tetramethylene diradical, which then moves on its lowest excited-state potential energy surface. After ∼240 fs, the diradical decays to its electronic ground state, because of electronic transitions induced by nonadiabatic coupling between the LUMO and HOMO. The diradical subsequently moves on its ground-state potential energy, with rotation about the central C−C bond. Cleavage of the second C−C bond—i.e., dissociation into two ethylene molecules—occurs at ∼400 fs in our simulations. We have found that the C−C−C−C torsional angle is an important internal coordinate during the reaction, but C−C−C bond bending also has a key role in shaping the potential energy surface for the tetramethylene intermediate.

Acknowledgment. Acknowledgment is made to the donors of The American Chemical Society Petroleum Research Fund for support of this research at Nicholls State University. The authors also acknowledge support by the Research Fund of Chongqing University of Posts and Telecommunications, China (Grant A2006-81), the Natural Science Foundation Project of CQ CSTC, China (Grant No.2006BB2367), the National Natural Science Foundation of China (Grant 20473060), and the Robert A. Welch Foundation (Grant A-0929). The Supercomputer Facility at Texas A&M University provided computational assistance.

References and Notes

(1) Woodward R.; Hoffmann, R. B. *The Conservation of Orbital Symmetry*; Academic Press: New York, 1970.
(2) Berson, J. *Science* **1994**, *266*, 1338 and references therein.
(3) Gerberich, H. R.; Walters, W. D. *J. Am. Chem. Soc.* **1961**, *83*, 39351.
(4) Gerberich, H. R.; Walters, W. D. *J. Am. Chem. Soc.* **1961**, *83*, 4884.
(5) Dervan, P. B.; Uyehara, T. *J. Am. Chem. Soc.* **1976**, *98*, 1262.
(6) Dervan, P. B.; Uyehara, T. *J. Am. Chem. Soc*. **1979**, *101*, 2076.
(7) Dervan, P. B.; Uyehara, T.; Santilli, D. S. *J. Am. Chem. Soc*. **1980**, *102*, 3863.
(8) Scacchi, G.; Richard, C.; Back, M. H. *Int. J. Chem. Kinet.* **1977**, *9*, 513.
(9) Pedersen, S.; Herek, J. L.; Zewail, A. H. *Science* **1994**, *266*, 1359.
(10) Polanyi, J. C.; Zewail, A. H. *Acc. Chem. Res.* **1995**, *28*, 119.
(11) Borden, W. T.; Davidson, E. R. *J. Am. Chem. Soc.* **1980**, *102*, 5409.
(12) Bernardi, F.; Bottoni, A.; Robb, M. A; Schlegel, H. B.; Tonachini, G. *J. Am. Chem. Soc.* **1985,** *107*, 2260.
(13) Bernardi, F.; Bottoni, A.; Celani, P.; Olivucci, M.; Robb, M. A; Venturini, A. *Chem. Phys. Lett*. **1992**, *192*, 229.
(14) Doubleday, C. *J. Am. Chem. Soc.* **1993**, *115*, 11968.
(15) Doubleday, C. *Chem. Phys. Lett.* **1995**, *233*, 509.
(16) Doubleday, C. *J. Phys. Chem*. **1996**, *100*, 15083.
(17) Doubleday: C.; Bolton, K.; Peslherbe, G. H.; Hase, W. L. *J. Am. Chem. Soc*. **1996**, *118*, 9922.
(18) Moriarty, N. W.; Lindh, R.; Karlström, G. *Chem. Phys. Lett*. **1998**, *289*, 442.
(19) Houk, K. N.; Reno, B. R.; Nendel, M.; Black, K.; Yoo, H. Y.; Wilsey, S.; Lee, J. K. *J. Mol. Struct.: THEOCHEM* **1997**, *169*, 398−399.
(20) Feyter, S. D.; Diau, E. W. G.; Scala, A. A.; Zewail, A. H. *Chem. Phys. Lett.* **1999**, *303*, 249.
(21) Ventura, E.; Dallos, M.; Lischka, H. *J. Chem. Phys.* **2003**, *118*, 10963.
(22) Dou, Y.; Torralva, B. R.; Allen, R. E. *J. Mod. Opt.* **2003**, *50*, 2615.
(23) Dou, Y.; Torralva, B. R.; Allen, R. E. *Chem. Phys. Lett.* **2004**, *392*, 352.
(24) Graf, M.; Vogl, P. *Phys. Rev. B.* 1**995**, *51*, 4940. (See also Boykin, T. B.; Bowen, R. C.; Klimeck, G. *Phys. Rev. B* **2001**, *63*, 245314.)
(25) Porezag, D.; Frauenheim, Th.; Köhler, Th.; Seifert, D.; Kaschner, R. *Phys. Rev. B* **1995**, *51*, 12947.
(26) Torralva, B. R.; Niehaus, T. A.; Elstner, M.; Suhai, S.; Frauenheim, Th.; Allen, R. E. *Phys. Rev. B* **2001**, *64*, 153105.
(27) Dou, Y.; Allen, R. E. *J. Mod. Opt.* **2004**, *51*, 2485.
(28) Allen, R. E.; Dumitrica, T.; Torralva, B. R. In *Ultrafast Physical Processes in Semiconductors*; Tsen, K. T., Ed.; Academic Press: New York, 2001; Chapter 7.
(29) Wang, Y.; Suo, B.; Zhai, G.; Wen, Z. *Chem. Phys. Lett*. **2004**, *389*, 315.